ACS OMEGA

Open Access

http://pubs.acs.org/journal/acsodf

Article

Energy and Mass Matching Characteristics of the Heat-Absorbing Side of the Ammonia Energy Storage System under Nonuniform Energy Flow Density

Kang Chen,* Yiming Jin, Huaiwu Peng, Pengfei Chen, Junfeng Zhang, Zhi Zhou, and Yueshe Wang

Cite This: *ACS Omega* 2023, 8, 33321−33331

Read Online

ACCESS | Metrics & More | Article Recommendations

ABSTRACT: Ammonia thermochemical energy storage is based on a reversible reaction and realizes energy storage and utilization by absorbing and releasing heat. Under different energy flow densities, the efficiency of an ammonia reactor composed of multiple ammonia reaction tubes is different. Based on the coupling model of light, heat, and chemical energy of an ammonia decomposition reaction system, taking a 20 MW solar thermal power plant as the research object, this paper proposes a new model of ammonia energy storage system, which places the ammonia decomposition side in a low-pressure environment and the ammonia synthesis side in a high-pressure environment. The effects of different inlet temperatures, inlet flow rates, flow distribution, and energy flow density distribution on the ammonia energy storage system were studied. The results show that the increase of inlet temperature and the decrease of inlet flow rate are beneficial to the improvement of thermal efficiency and exergy efficiency of the system to a certain extent, but when the inlet temperature increases or the inlet flow rate decreases to a certain extent, the efficiency of the system will decline. Under the condition of nonuniform energy flow density and nonuniform inlet flow distribution, more ideal system thermal efficiency and exergy efficiency can be obtained.

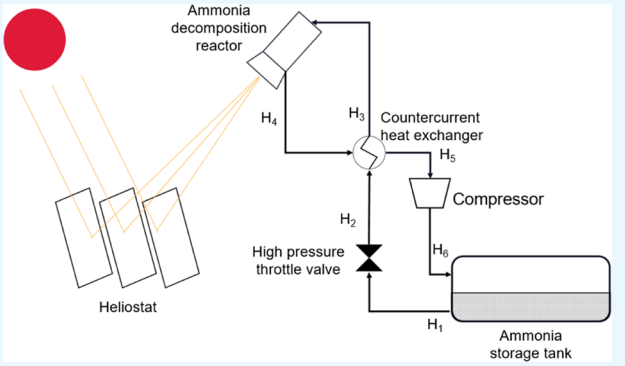

1. INTRODUCTION

In terms of energy structure, China is a typical country with "rich coal, poor oil, and little gas", and its total energy consumption ranks first in the world.[1] In China, the contradiction between increasing energy consumption and unreasonable energy consumption mode and consumption structure is becoming increasingly prominent. We are facing an unprecedented energy crisis. At this stage, China is vigorously promoting the adjustment and transformation of the energy structure, investing a lot of energy in the field of new energy and promoting the realization of the "carbon peaking and carbon neutrality goals". Compared with other kinds of new energy, research in the field of solar energy has made rapid progress.[2] At the same time, considering the construction cost, solar energy is the cheapest and most abundant new energy. According to the national electric power industry data[3] in 2020 according to the statistics of the National Energy Administration of China, thermal power generation accounted for 56.6%, hydropower generation accounted for 16.2%, nuclear power generation accounted for 2.3%, wind power generation accounted for 12.8%, and solar power generation accounted for 11.5%. Among the above power generation technologies, the year-on-year growth of wind power and solar power generation was 34.6% and 24.1%, respectively.[4] It can be seen that solar power generation is steadily increasing, and the prospect of solar power generation is bright. At present, solar power generation technology is divided into photovoltaic power generation and thermal power generation. The main problem of solar power generation is discontinuity. Photothermic power generation can store part of the heat exceeding the rated power generation capacity by matching it with the energy storage system.

Photothermic power generation gathers light on the heat collector to heat the medium and drive the turbine. If the heat is sufficient, the heat will be stored by sensible heat, latent heat, and chemical energy. In the photothermic power generation system, adding an energy storage system can make the operation of the power generation system more stable and improve the economy. Thermochemical energy storage has the advantages of high mass density, high energy storage efficiency, little heat loss, and low operating temperature. Compared with

Received: April 10, 2023
Accepted: July 24, 2023
Published: September 7, 2023

sensible heat storage and latent heat storage, the energy density of thermochemical energy storage is 10−100 times higher.[5] For thermochemical energy storage, both products and reactants can be stored at ambient temperature or operating temperature.[6] Thermochemical energy storage has wider application prospects in the future. Nowadays, there are mainly five kinds of thermochemical energy storage systems, among which the ammonia thermochemical system has great potential with fewer side reactions, lower reaction temperature, and higher controllability.

At present, there are few studies on ammonia thermochemical energy storage in the world, especially on building a complete ammonia thermochemical energy storage system. In the 1970s, the Australian National University (ANU) began to study ammonia thermochemical energy storage and applied it to solar photothermal power generation. Carden[7] was the earliest proponent. Williams et al. of ANU[8] calculated the efficiency of ammonia thermochemical energy storage in 1979. If the degree of ammonia decomposition exceeds 60%, then 90% of the energy storage efficiency can be obtained.

Kanamori et al.[9] studied the thermochemistry energy storage of the $CaO/Ca(OH)_2$ system. The heat release rate, heat output, and thermal efficiency were studied by using heat storage devices and finned heat exchangers. A Meier[10] used CFD to simulate the tower solar reactor with thermochemistry energy storage. Bogdanovi et al.[11] explored the operating temperature of the thermochemistry energy storage system and tested its stability under multiple cycles, and by means of combined TEM−EDX investigations, the mechanism was elucidated at the nanoscale.

In 1998, Luzzi et al. of ANU[12] proposed the ammonia photothermic energy storage system. The system is mainly divided into three parts, namely, the focusing system, heat collection system, and exothermic system. The sun is focused on the ammonia decomposition reactor through the mirror field, and ammonia dissociation is promoted by photothermic heating. In the heat collection part, the mixture of hydrogen and nitrogen generated by the ammonia decomposition reactor flows through the countercurrent heat exchanger to heat the ammonia in another channel and then returns to the ammonia storage tank. The ammonia in the tank exists in the form of liquid, so liquid ammonia and mixed gas can be separated automatically. The liquid ammonia in the tank is at the bottom, and the mixed gas is at the top. Ammonia is pumped out from the bottom and heated into ammonia(g) by the mixed gas at the outlet of the ammonia decomposition reactor after passing through the countercurrent heat exchanger. The ammonia enters the ammonia decomposition reactor to realize circulation of the heat collection part. In the heat release part, the mixed gas is pumped out from above, heated into high-temperature gas through the countercurrent heat exchanger, and then delivered to the synthesizer. In the synthesizer, as synthetic ammonia is an exothermic reaction, it can generate electricity through subsequent utilization of heat. The heat released can heat water to generate superheated steam, drive the Rankine cycle of steam, and generate electric energy. The synthesis and dissociation systems can realize the process of energy storage and utilization through a reversible ammonia synthesis reaction.

In 1998, Lovegrove et al.[13] built the first 1.1 kW ammonia solar thermochemical energy storage closed-loop system, which includes ammonia dissociation process and ammonia synthesis process. A 20 m^2 dish condenser was used for heating, demonstrating the feasibility of using solar photothermic power generation for 24 h. They also evaluated the system, which was expected to achieve a 15 kW operation. The scheme was to use an ammonia decomposition reactor consisting of 20 reaction tubes, while the ammonia synthesizer consisted of 19 tubes. The synthesis device verified the simulation results of Richardson et al.

In 2004, Lovegrove et al.[14] built a 15 kW ammonia thermochemical energy storage system on this basis. They verified the feasibility of realizing the operation of the ammonia thermochemical energy storage system on a large scale, and its energy storage efficiency reached 53%. And according to Lovegrove's research, it shows that in the ammonia energy storage device, the most important parameter for the reactor is the average temperature of the reaction tube. If the average temperature is slightly higher than the output temperature, then the performance was optimal at this time.

In 2012, Rebecca[15] used the ray tracing method to calculate the solar flux density distribution of the dish condenser on the reaction tube of the cavity heat receiver on the basis of the previous work. Then, the influence of different absorber taper angles and Solar zenith angles on the conversion efficiency of solar energy to chemical energy of the whole system was analyzed, and the thermal efficiency of the reactor was deduced.

In 2017, Chen et al., on the basis of Lovegrove's previous research, conducted a follow-up study.[16,17] Concentric pipes are used as ammonia synthesizers to heat water vapor from 350 °C at the inlet to 650 °C at the outlet in a supercritical state. This state enables steam to complete the Rankine cycle. Therefore, a Rankine cycle system can be installed behind the ammonia thermochemical energy storage system to achieve the purpose of power generation. In addition, in the process of ammonia synthesis, the heat transfer process of the reaction is most sensitive to the activation energy, and the constant related to the reaction rate has less influence on the heat transfer process. At the same time, the research results show that improving the heat transfer capacity and reducing the inlet ammonia mass fraction are the key to improving the steam mass flow capacity of the reactor for the heating unit syngas mass flow.

Masci[18] proposed a medium-temperature ammonia decomposition system for the previous high-temperature ammonia decomposition reactor, which makes good use of the medium-temperature environment of about 923 K generated by focused solar energy, and improves the energy conversion rate. Abdiwe and Haider[19] established a one-dimensional transient model to study the effect of flow rate on the efficiency of ammonia decomposition tube and ammonia synthesis reaction tube. Long et al.[20] established the mathematical model of Exothermic reaction (ammonia synthesis reactor), quantitatively analyzed and discussed the influence of inlet air temperature and flow rate on the reaction under certain pressure and hydrogen nitrogen ratio, gave the operating parameters to achieve exergy optimization and heat energy maximization, and compared the relationship between optimal exergy and maximum heat energy. Villafan-Vidales et al.[21] used FLUENT to simulate the reversible reaction of two-dimensional metal oxides under the condition of focused solar energy and studied the effects of solar radiation, porosity, and flow rate on the temperature distribution in a porous medium. Wang et al.[22] studied methane reforming and obtained the temperature distribution of gas and solid in a porous medium

https://doi.org/10.1021/acsomega.3c02426
ACS Omega 2023, 8, 33321−33331

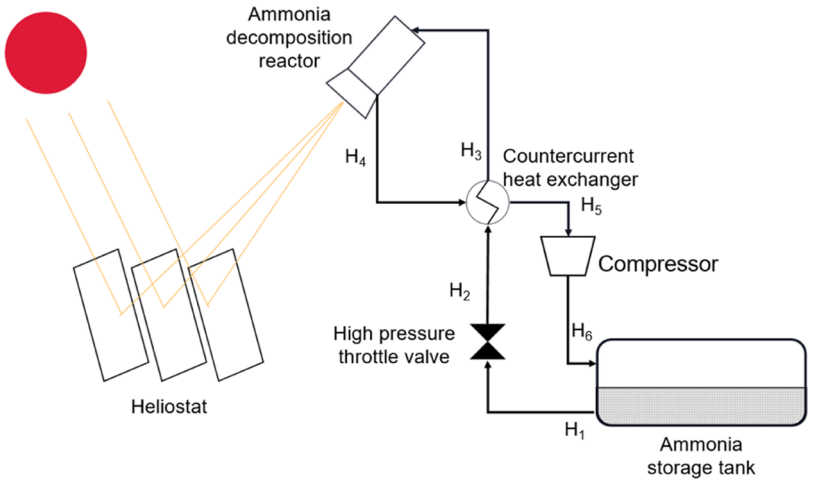

Figure 1. Flowchart of heat absorption side.

by using the local nonequilibrium method. The boundary condition is the Gaussian distribution of the solar energy flow density.

In the study, taking the 20 MW photothermic power plant as the model, the model of the heat-absorbing side of the ammonia energy storage is built to obtain models of energy flow and mass flow. The effects of inlet temperature, flow distribution, and energy flow density distribution on the thermal efficiency and exergy efficiency of the heat-absorbing side of the amino energy storage system are studied, so as to completely establish the dynamic energy relationship from the ammonia reactor to the heat-absorbing side of the amino energy storage system.

2. SIMULATION AND EXPERIMENT

The energy storage system of a complete tower solar photothermic system includes the heat absorption side dominated by an ammonia decomposition reaction and the heat release side dominated by an ammonia synthesis reaction. The composition of the heat-absorbing side shall include a high-pressure throttle valve, compressor, ammonia decomposition reactor, ammonia storage tank, heat exchanger, and condensation separation device. Since the working pressure of the heat-absorbing side (5 MPa) is different from that of the heat-releasing side and the working pressure of the ammonia storage tank (15 MPa, 25 °C) is high, a high-pressure throttle valve and steam turbine are required. The flow diagram is shown in Figure 1. The heliostat focuses sunlight in the ammonia decomposition reactor, and the absorbed heat promotes the ammonia decomposition reaction. As the hydrogen and nitrogen formed by decomposition are in a high-temperature state, sensible heat can be used to heat the normal-temperature ammonia gas from the ammonia storage tank, which is more conducive to the ammonia decomposition reaction. More heat can be stored in the form of chemical energy. Then, the decomposed mixed gas is put into the ammonia storage tank again through the compressor. The decomposition reaction cannot be carried out completely, so there is ammonia in the mixture besides 3:1 H_2−N_2. The critical parameters of the three gases are shown in Table 1:

Therefore, based on the pressure assumed previously, ammonia will be liquid in a certain range and gaseous in other ranges. The relationship between the ammonia condensation temperature and saturation pressure is shown in Figure 2. When the temperature rises, the saturation pressure of ammonia increases. When the temperature changes from 273.15 K (0 °C) to 403.15 K (130 °C), the pressure changes from 0.43 to 10.9 MPa. At the same time, when the ammonia is in the mixed state, the partial pressure of ammonia in A state is greater than the saturation pressure of ammonia or the temperature is lower than the condensation temperature, the gaseous ammonia will be condensed into liquid ammonia. When ammonia is in state B, that is, when the partial pressure of ammonia is less than the saturation pressure of ammonia or the temperature is higher than the condensation temperature, the gaseous ammonia is still in the gaseous state of overheating. Therefore, in the high-pressure ammonia storage tank, ammonia can form a liquid, which can be automatically separated from hydrogen and nitrogen. The liquid ammonia extracted from the ammonia storage tank, after passing through the high-pressure throttle valve, decreases in pressure and becomes a relatively low-pressure ammonia gas for subsequent reaction.

Table 1. Critical Parameters for H_2, N_2, and NH_3

gas	critical temperature (°C)	critical pressure (MPa)
NH_3	135.2	11.3
H_2	−240	3.39
N_2	−147.05	3.39

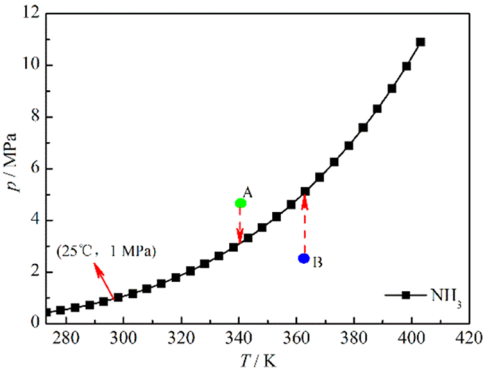

Figure 2. Relation between the ammonia saturation pressure and condensation temperature.

https://doi.org/10.1021/acsomega.3c02426
ACS Omega 2023, 8, 33321−33331

2.1. Ammonia Decomposition Reaction Tube Model.

In the reaction tube studied in this experiment, the diameter of the reaction tube is D, the wall thickness is b, the tube length is L, the interior is filled with NiO-Al_2O_3, the particles are uniform, and the average diameter is d_p. The ammonia gas flowing into the reaction tube will be gradually decomposed into hydrogen and nitrogen under the action of the catalyst. When the ammonia reactor is assembled, the ammonia reaction tubes are placed in parallel. Therefore, for a single reaction tube, the solar radiation surface is only half of the tube circumference, and the other half is assumed to be adiabatic.

Tamaru et al. studied the ammonia decomposition mechanism using tungsten as the catalyst. They concluded that when the ammonia pressure is in the high-pressure state, the reaction is a zero-order reaction, while when the ammonia pressure is in the low-pressure state, the reaction is a first-order reaction.[23] Therefore, according to the reaction kinetics, the Temkin−Pyzhev calculation equation is used to calculate the reaction rate R' in the process of the ammonia decomposition reaction

$$R' = k_0 \exp\left(-\frac{E_a}{RT_f}\right)\left[P_{N_2}K_p{}^2\left(\frac{P_{NH_3}{}^3}{P_{H_2}{}^3}\right)^{\alpha} - \left(\frac{P_{NH_3}{}^2}{P_{H_2}{}^3}\right)^{1-\alpha}\right] \quad (1)$$

where α is the empirical value, usually in the range of 0.5−0.75.[24]

To facilitate the calculation, the following assumptions are made:

(1) The catalyst particles are uniformly distributed in the reaction tube wall, the porosity is the same everywhere, and the thermal conductivity is constant.

(2) The reaction tube has a large length−diameter ratio, ignoring the influence of radial upward diffusion, and only considering the axial and circumferential diffusion.

(3) During the process of flowing through the catalyst, the ammonia gas is close to laminar flow, ignoring the radial and circumferential flow, and only considering the axial flow of the pipe.

(4) Because the reaction temperature of ammonia decomposition is not very high (500−600 °C), according to the research of Chen et al.,[25] it can be found that the deviation is less than 4.5% when the radiation in the tube is not considered. Therefore, the radiation heat transfer between particles and between particles and gas is ignored in this model.[26]

So, when the ammonia mass exchange is in equilibrium

$$\rho_f u_f \frac{\partial \omega_f}{\partial Z} = R'M_{NH_3} + \varepsilon\rho_f D_f\left(\frac{\partial^2\omega_f}{\partial r^2} + \frac{\partial\omega_f}{\partial r}\frac{1}{r} + \frac{\partial^2\omega_f}{\partial\theta^2}\frac{1}{r^2}\right) \quad (2)$$

In the above equation, the left-hand side is the change of the ammonia mass fraction in the control volume, the first term on the right-hand side is the ammonia mass fraction that changes with the reaction, and the second term on the right-hand side is the ammonia mass fraction that diffuses in the circumferential and radial directions.

Similarly, according to the above assumptions, when in the steady state, the following thermal equilibrium is established when using the local nonthermal equilibrium method for analysis

$$1 - \varepsilon\lambda_s\left(\frac{\partial^2 T_{solid}}{\partial r^2} + \frac{\partial T_{solid}}{\partial r}\frac{1}{r} + \frac{\partial^2 T_{solid}}{\partial\theta^2}\frac{1}{r^2}\right) = h_{sf}A(T_{solid} - T_f) \quad (3)$$

$$\rho_f u_f C_p \frac{\partial T_f}{\partial Z} = h_{sf}A(T_{solid} - T_f) - R'M_{NH_3}\Delta H + \varepsilon\lambda_f\left(\frac{\partial^2 T_f}{\partial r^2} + \frac{\partial T_f}{\partial r}\frac{1}{r} + \frac{\partial^2 T_f}{\partial\theta^2}\frac{1}{r^2}\right) \quad (4)$$

Table 2 shows the initial condition and boundary conditions of the model, and Table 3 shows the main parameter settings for numerical simulation:

Table 2. Initial Condition and Boundary Condition of the Ammonia Reaction Pipe

governing equation	initial condition	boundary condition
mass equation	$\omega_f(r,\theta,0) = 1$	$\frac{\partial\omega_f}{\partial r} = 0$
energy equation	$T_f(r,\theta,0) = T_{in}$	$q_w = -\varepsilon\lambda_f\frac{\partial T_f}{\partial r} - (1-\varepsilon)\lambda_s\frac{\partial T_{solid}}{\partial r}$ $(-0.5\pi \le \theta < 0.5\pi)$[26]
	$\frac{\partial T_{solid}(r,\theta,0)}{\partial r} = 0$	$\frac{\partial T_f}{\partial r} = \frac{\partial T_{solid}}{\partial r} = 0$ $(0.5\pi \le \theta < \pi, -\pi < \theta < -0.5\pi)$[26] $T_{solid} = T_f$

Table 3. Main Parameter Settings for Numerical Simulation

d_p (m)	ε	inlet temperature (°C)	outlet pressure (MPa)	inlet flow rate ($g\cdot s^{-1}$)
10^{-3}	0.5	200	2	17

At the pipe wall, there is thermal equilibrium

$$q_w = \xi q_t - q_s \quad (5)$$

$$q_s = h_a(T_{solid} - T_a) + \chi\sigma(T_{solid}{}^4 - T_a{}^4) \quad (6)$$

When the tower solar power station is located in Beijing, the annual average daily solar irradiance on the horizontal plane is 15261.14/kJ·m^{-2}·d^{-1}, and the height angle at the noon of the spring equinox is 50°. The energy flow density of the sunlight after focusing through the mirror field can be written as

$$q_t = \frac{P_h}{2\pi\sigma_{HF}}e^{x^2+z^2/2\sigma_{HF}{}^2} \quad (7)$$

The heat projected by the solar energy on the outer wall of the tube is transferred to the porous solid particles through the tube wall. After that, heat is transferred from solid particles to fluid in the form of convective heat transfer. Wakao equation[27] is adopted for the convection heat transfer equation

$$h_{sf} = \frac{\lambda_f(2 + 1.1Pr^{0.33}Re^{0.6})}{d_p} \quad (8.1)$$

$$A = \frac{6(1-\varepsilon)}{d_p} \quad (8.2)$$

As the reaction proceeds, the pressure at each position in the reactor is different, and the fluid parameters at each position, such as thermal conductivity, viscosity, and density, will also

https://doi.org/10.1021/acsomega.3c02426
ACS Omega 2023, 8, 33321−33331

change. Assuming that the reaction pipe is a fixed bed, the pressure drop can be calculated by using the Eugen equation

$$\frac{\Delta P}{L} = 150\frac{(1-\varepsilon)^2}{\varepsilon^3 {d_p}^2}\mu u_f + 1.75\frac{1-\varepsilon}{\varepsilon^3}\frac{\rho {u_f}^2}{d_p} \quad (9)$$

We use the Temkin−Pyzhev equation (eq 1) to calculate the reaction rate R'. The large mass fraction of ammonia in the reaction is the dominant factor in the concentration of reaction kinetics. Therefore, when calculating the reaction rate, it is considered that the reaction rate is mainly related to the partial pressure of ammonia, so the second term is ignored. After eq 1 is simplified, a new reaction rate equation can be obtained

$$R' = k_0 e^{-E_a/kT_f} P_{NH_3} \quad (10)$$

2.2. Model Validation. For the simulation model of the ammonia decomposition reactor, the grid independence was verified. Based on the 10 m ammonia decomposition reaction tube, the grid division of the cross section shall be considered first. The grid of the cross section was divided into 5 × 5, 20 × 20, 30 × 30, 40 × 40, and 50 × 50. At this time, assuming that there are 200 grids in the axial direction, the ammonia mass fraction at the outlet center can be obtained, as shown in Figure 3. When the cross section grid division was greater than

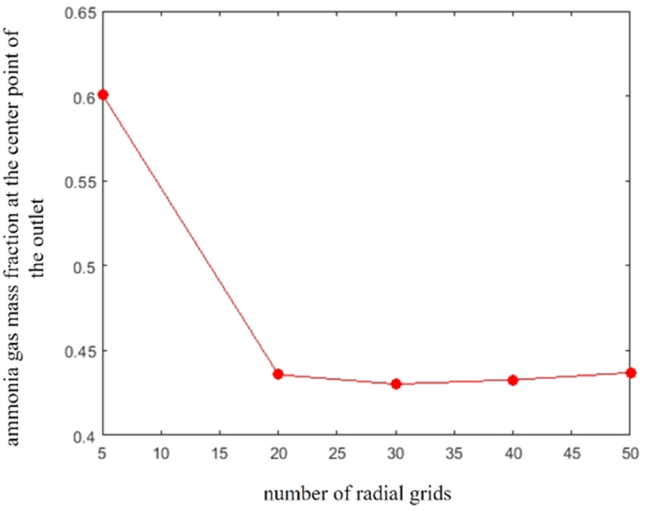

Figure 3. Grid independence verification (cross section).

20 × 20, the ammonia mass fraction at the outlet center had little change, so the cross section grid division was selected as 20 × 20. For axial grid generation, the grid generation based on cross section is 20 × 20, and the number of grids selected was 10, 20, 50, 100, 200, 300, 400, 500, and 1000. The results are shown in Figure 4. It can be seen from the figure that when the number of grids in the axial direction is 500, the increase in the number of grids has little effect on the ammonia mass fraction at the outlet center. To sum up, the grid of ammonia decomposition reaction tube is finally divided by 20 × 20 × 500.

At the same time, an experimental platform was built to compare the error between the real experimental value and the numerical simulation value. The experimental platform is shown in Figure 5. The ammonia decomposition heat absorption experimental platform mainly consists of three major components: an ammonia reaction open-cycle system, an electric heating system, and a data acquisition system. The

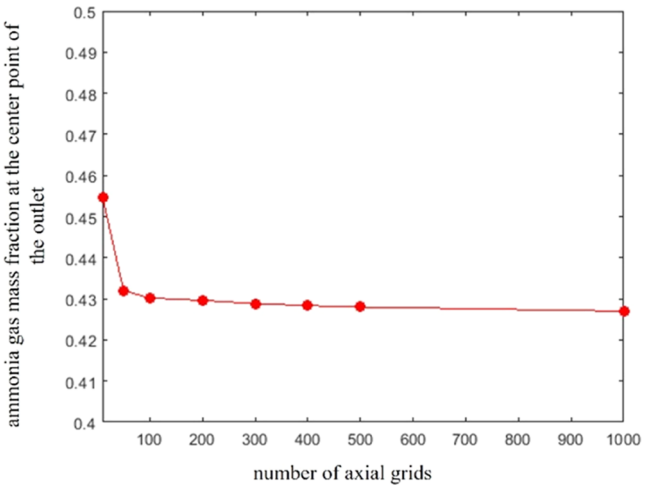

Figure 4. Grid independence verification (axial).

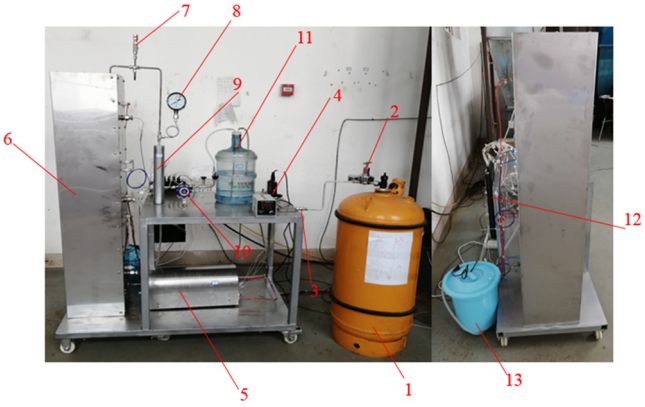

Figure 5. Ammonia decomposition experimental platform. (1) Ammonia storage tank; (2) pressure-reducing valve; (3) filter; (4) mass flow controller; (5) preheater; (6) ammonia reactor; (7) pressure relief valve; (8) pressure gauge; (9) condenser; (10) back pressure valve; (11) absorber; (12) IMP data collector; (13) condensate water tank.

ammonia reaction open-cycle system includes an ammonia storage tank, a flow controller, a reaction tube, auxiliary instruments at the front end of the reaction, a cooling device at the back end of the reaction, a back pressure valve, and a tail gas treatment container. The pipeline is composed of 316 stainless steels with an outer diameter of 8 mm and a wall thickness of 2 mm, and other geometric parameters of the connecting parts are based on this. The effective reaction length of the ammonia reaction tube is 1 m, the inner diameter is 30 mm, and the wall thickness is 10 mm.

The experimental platform was set to work under normal pressure; the inlet temperature was 50 °C; the pipe length was 10 m; the wall thickness was 10 mm; and the inner diameter was 30 mm. The porosity of the porous medium (catalyst) was taken as 0.5. It can be seen from Figure 6 that the gap is relatively large at low flow rates. But the values agree well at relatively high flow rates, with errors within ±10%. The reason for the large error at a low flow rate may be that the pipe wall temperature is more susceptible to the external environment, and the pipe wall temperature is not completely evenly distributed, while the simulation process always keeps the pipe wall temperature constant. In the following simulation, the flow rate of ammonia is relatively high, so this model can better

https://doi.org/10.1021/acsomega.3c02426
ACS Omega 2023, 8, 33321−33331

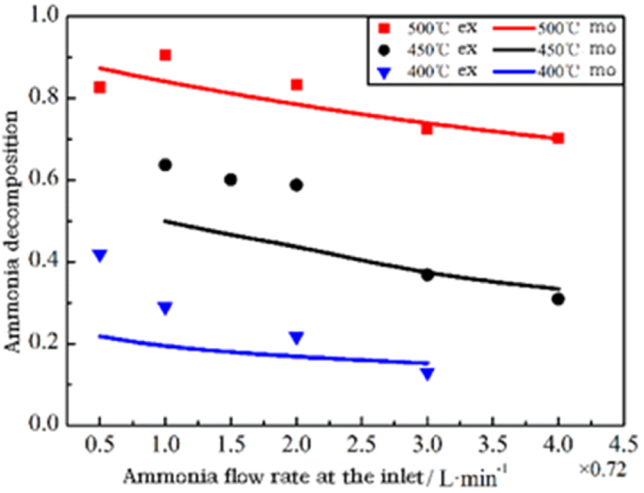

Figure 6. Difference between numerical simulation and experimental data.

simulate the process of the ammonia-catalyzed reaction, to verify the adaptability of the model.

2.3. Ammonia Reactor Model. As described in Section 2.1, the structure of the ammonia reactor should be as shown in Figure 7. After the sunlight is focused through the heliostat,

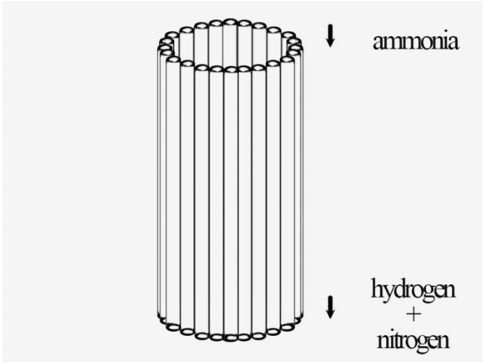

Figure 7. Schematic diagram of the ammonia reactor model.

it will focus on the inner wall of the reaction tube, and the tube wall will absorb heat to carry out the ammonia decomposition reaction.

In the establishment of the ammonia reactor model, the model established in Section 2.1 is used for each ammonia reaction pipe. The ammonia reactor is approximately a cylinder, and the diameter of the reaction pipe is negligible relative to the diameter of the reactor. The diameter of the reactor model is 8.5 m, and there are 800 reaction tubes in total. Because the heat flow density is symmetrical and the reaction tubes are symmetrical, only half of the 800 tubes can be studied. And in terms of the distribution of pipe inlet flow, this article proposes three different inlet flow distributions, as shown in eqs 11−13. No matter how the flow distribution changes, the total flow rate through all pipes remains unchanged at 14 kg·s^{-1}.

$$q_{m1,i} = \text{constUniform distribution} \tag{11}$$

$$q_{m2,i} = 1.1q_{m1,i} - 0.2\frac{q_{m1,i}}{400-1}(i-1)\text{Linear distribution1} \tag{12}$$

$$q_{m3,i} = 1.2q_{m1,i} - 0.4\frac{q_{m1,i}}{400-1}(i-1)\text{Linear distribution2} \tag{13}$$

where i is the number of tube.

The generating power of the power station is 20 MW. Assuming that the efficiency of the solar tower power generation unit is 42%, the heat absorbed is about 47.62 MW. At the same time, the efficiency of the heat absorption device is assumed to be 80%. Therefore, in order to meet the power generation, the input solar q_t should be 59.50 MW. Assuming that the ammonia decomposition rate is 90% and the reaction heat of ammonia decomposition is 54 kJ·mol^{-1}, the total flow of ammonia can be roughly calculated as 1 kmol·s^{-1}, that is, the mass flow is about 17 kg·s^{-1}. In the loop, the flow loss is ignored, and the efficiency of the countercurrent heat exchanger is assumed to be 95%. The working pressure in the ammonia storage tank is 15 MPa, and the pressure in the heat absorption circuit is 5 MPa.

The enthalpy at the inlet of the ammonia decomposition reactor is H_3. According to the relationship between the enthalpy value of ammonia and the temperature at 5 MPa

$$h_{NH_3} = 360.71 + 5.42723T - 0.00573T^2 + 3.88\times10^{-6}T^3\frac{\text{kJ}}{\text{kg}} \tag{14}$$

H_3 is obtained. Based on the modeling in Section 2.1, the temperature, ammonia mass fraction, and outlet enthalpy H_4 of 400 ammonia reaction tubes in different positions are calculated.

The outlet of the ammonia tank is liquid ammonia, assuming the chemical enthalpy H_1 is 0. After liquid ammonia flows out of the ammonia storage tank, it passes through the throttle valve first. The process in the throttle valve is regarded as an adiabatic process, only reducing the pressure without changing the enthalpy value, so H_2 and H_1 are equal.

Therefore, the enthalpy of the cold and hot end inlets of the counter-flow heat exchanger in the exothermic circuit have been determined, and then according to the heat exchange characteristics of the counter-flow heat exchanger

$$(H_3 - H_2)\times q_m = (H_4 - H_5)\times q_m \times 95\% \tag{15}$$

H_5 can be obtained.

After the reaction gas goes out from the hot end of the countercurrent heat exchanger, it enters the compressor, which compresses the 5 MPa gas into 15 MPa, and its work is

$$W_{c,J} = 2\frac{n}{n-1}RT_5q_m(\Pi^{n-1/n} - 1) \tag{16}$$

where π is the compressor pressure ratio

$$\Pi = \left(\frac{p_6}{p_5}\right)^{1/2} \tag{17}$$

The difference between H_5 and H_6 is the work done by the compressor. In the whole heat absorption circuit, the enthalpy values are marked in Figure 8:

For the ammonia synthesis circuit, the energy storage efficiency is defined as

$$\eta_{st} = \frac{H_6 - H_1}{Q_{in}} \tag{18}$$

https://doi.org/10.1021/acsomega.3c02426
ACS Omega 2023, 8, 33321−33331

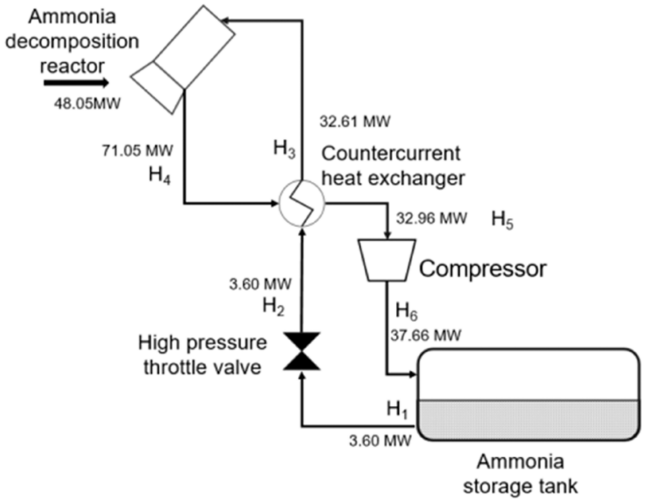

Figure 8. Enthalpy of the heat absorption loop.

It can be calculated by substituting the data that the energy storage efficiency of a solar tower power station equipped with an amino energy storage device was 86.3%. The efficiency of sensible heat energy storage is 75%.[28] By contrast, the efficiency of thermochemical amino energy storage has been significantly improved.

The efficiency of the heat absorption circuit is defined as

$$\eta_{ab} = \frac{H_6 - H_1}{Q_{in} + W_{c,J}} \tag{19}$$

The efficiency of the loop is 64.4%.

The exergy efficiency can be expressed as the total exergy input compared to the stored exergy, which includes the exergy input on the reaction tube and the work performed by the compressor. It can be expressed as

$$\eta_{ex} = \frac{q_m(1-\omega)(\Delta H - T_0 ds)}{E_{x,s} + W_{c,J}} \tag{20}$$

3. RESULTS AND DISCUSSION

3.1. Influence of Different Inlet Temperatures on System Performance. This section studied the influence of different inlet temperatures and flow rates on system performance. Figure 9 shows the ammonia decomposition rate and pipe wall peak temperature of reaction tubes with inlet temperatures of 473, 573, and 673 K, respectively. From the figure, it can be clearly seen that the ammonia decomposition rate at the outlet of the reaction tube gradually decreases along the direction of the reaction tube arrangement, and the decreasing speed gradually becomes faster. At the same time, the distribution of ammonia decomposition rate is similar to the distribution of solar energy flow density. In addition, it was also found from the figure that with the increase of inlet temperature, the ammonia decomposition rate of each reaction tube and the peak temperature of the tube wall are increasing, leading to the increase of the ammonia decomposition rate of the total system. In addition, the heat loss of the ammonia reactor will also increase, as shown in Table 4.

Table 4 shows the simulation results of the system performance and energy consumption of each module under three inlet temperatures. During the circulation, there is a cooling heat loss, and when the reaction gas returns to the ammonia storage tank, the temperature is higher than the storage temperature. Therefore, this part of the heat is considered as total loss. It can be seen from the table that with the increase of inlet temperature, ammonia conversion rate and system thermal efficiency increase. As the ammonia decomposition rate of the system is improved, the energy consumption of the compressor will increase. The increase of inlet temperature makes it possible to absorb most of the heat in the reaction and transfer it to the ammonia to be decomposed, thus greatly reducing the cooling heat loss. Although the increase of inlet temperature leads to a small increase in the reactor heat loss and compressor energy consumption, the overall energy loss decreases, so the system efficiency increases. At the same time, it can be seen that when the inlet temperature rises to 673 K, the exergy efficiency of the system decreases. The reason is that the ammonia temperature at the inlet is too high, and the preheating device (heat exchanger) is no longer able to meet the demand. Therefore, additional heat sources are needed for heating, resulting in an increase in the energy consumption of the entire system.

Figure 10 shows the change in the thermal efficiency and exergy efficiency of the system with the inlet temperature. It can be seen that the thermal efficiency of the system increases with the increase of temperature. However, the exergy efficiency of the system increased first and then decreased with the increase of temperature. The exergy efficiency of the system plays a decisive role in the level of energy quality and power generation. Therefore, the inlet temperature should maximize the exergy efficiency of the system. In this example,

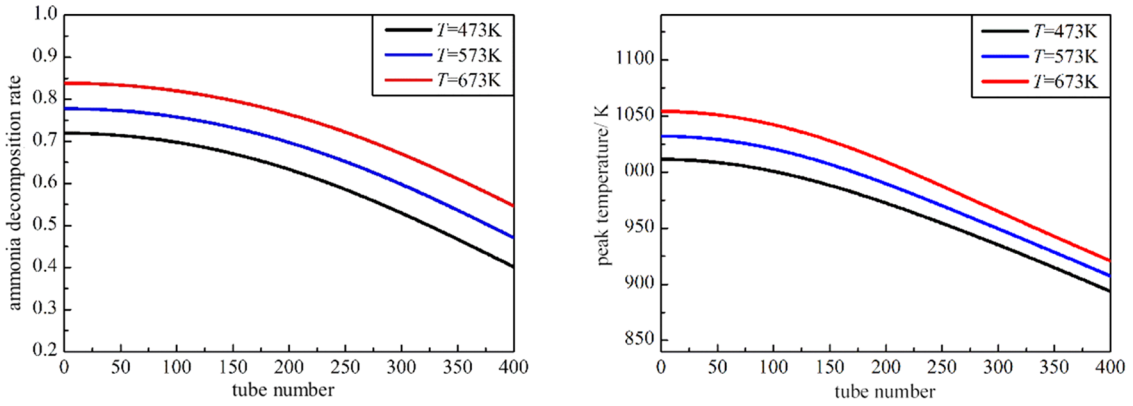

Figure 9. Distribution of the ammonia decomposition rate (left) and pipe wall peak temperature (right) at different inlet temperatures.

https://doi.org/10.1021/acsomega.3c02426
ACS Omega 2023, 8, 33321−33331

Table 4. System Efficiency at Different Inlet Temperatures

inlet temperature (K)	ammonia decomposition rate	thermal efficiency	exergy efficiency	reactor heat loss (MW)	cooling heat loss (MW)	energy lost by compressor (MW)
473	60.75%	63.89%	58.49%	8.311	10.11	4.008
573	67.17%	68.51%	60.64%	9.223	6.364	4.431
673	73.91%	70.38%	59.79%	9.812	5.319	4.876

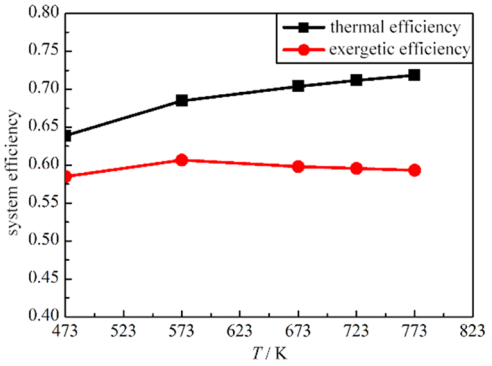

Figure 10. System efficiency changes with temperature.

the inlet temperature of 573 K was the optimal design temperature.

3.2. Influence of Different Inlet Flow on System Performance. Then, the impact of different flow rates (uniform distribution) on the system performance was simulated. Figure 11 shows the ammonia decomposition rate and pipe wall peak temperature of different reaction tubes in the ammonia reactor at different inlet flow rates. From Figure 11, it can be seen that with the increase of inlet flow rate, the ammonia decomposition rate and pipe wall peak temperature of each reaction pipe decrease, so the ammonia decomposition rate of the total system will decrease and the loss will also decrease with the reaction, as shown in Table 5.

The efficiency and loss of different parts at different flow rates are shown in Table 5. It can be seen that with the increase of inlet flow rate, ammonia decomposition rate, system thermal efficiency, and exergy efficiency are reduced. Among all of the heat losses, the cooling heat loss has the largest change, resulting in the reduction of reactor heat loss and compressor loss, and the system efficiency decreases. In terms of the total amount of ammonia converted, the total amount of ammonia converted is reduced, so the power consumption of the compressor can be reduced. For cooling heat loss, although the cooling heat loss per unit mass of ammonia decreases, the increase of inlet flow makes the cooling heat loss larger.

According to the data in Table 5 (simulated results), it can be predicted that when the flow is lower than a certain value, the flow is too small to store enough heat energy as chemical energy and the efficiency is too low; When the flow rate is higher than a certain value, the heat loss of the system is too large and the efficiency decreases. Figure 12 shows the change in system efficiency under different inlet flows. As the flow increases, the system efficiency first increases and then decreases. Therefore, for the amino energy storage system with tower solar thermal power generation, there is also an optimal flow condition. When the flow rate is small, due to the limitation of chemical reaction balance, the heat absorbed by the ammonia decomposition reaction cannot absorb enough solar energy; When the flow is large, more ammonia will only increase the sensible heat in the reaction tube, instead of being converted and stored in hydrogen and nitrogen in the form of chemical energy, so it will cause an excessive loss in the cooling process. According to the simulation in the figure, the optimal flow rate is about 14 $kg{\cdot}s^{-1}$.

The ammonia decomposition rate distribution of the reaction tube is closely related to the solar energy flow density distribution. The closer to the maximum value of nonuniform heat flux, the smaller the impact of temperature and flow on the ammonia decomposition rate. The reaction has reached equilibrium. No matter how much energy is input, the energy that can be converted has reached the limit, but at the same time, the reaction tubes at other locations have not yet reached the optimal conversion condition.

Figure 13 shows the pipe wall peak temperature distribution under three inlet flow distributions under the conditions of 473 K inlet temperature and 14 $kg{\cdot}s^{-1}$ inlet flow, respectively. It can be seen from the figure that the pipe wall peak temperature is smaller under the condition of nonuniform flow distribution, the peak wall temperature of linear distribution 1 is 20 K lower than that of uniform distribution, and the peak wall temperature of linear distribution 2 is 40 K lower than that

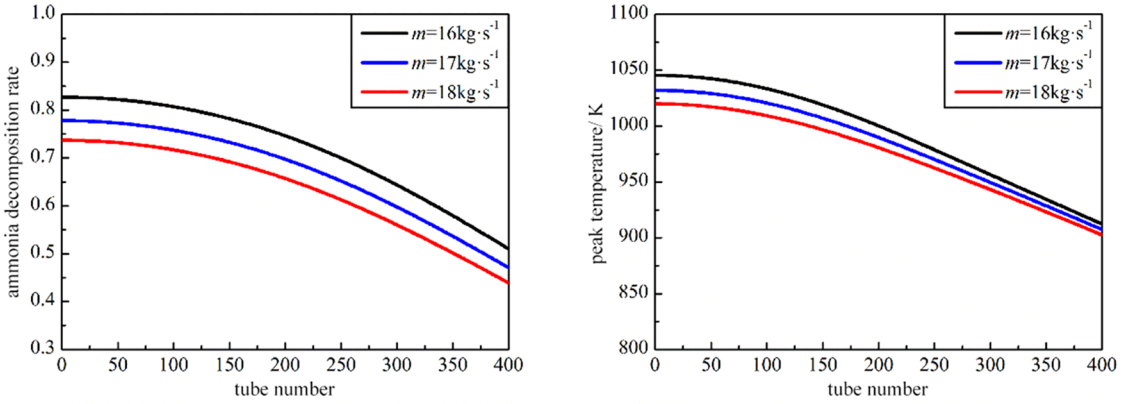

Figure 11. Distribution of ammonia decomposition rate (left) and pipe wall peak temperature (right) under different inlet flows.

https://doi.org/10.1021/acsomega.3c02426
ACS Omega 2023, 8, 33321−33331

Table 5. Comparison of System Efficiency Results under Different Inlet Flows

Inlet flow ($kg·s^{-1}$)	ammonia decomposition rate	thermal efficiency	exergy efficiency	reactor heat loss (MW)	cooling heat loss (MW)	energy lost by compressor (MW)
16	71.90%	69.78%	62.25%	9.313	5.299	4.465
17	67.17%	68.51%	60.64%	9.223	6.364	4.431
18	63.28%	67.64%	59.64%	8.912	7.376	3.905

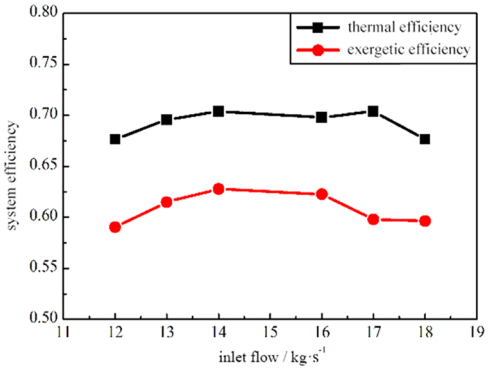

Figure 12. System efficiency changes with an inlet flow.

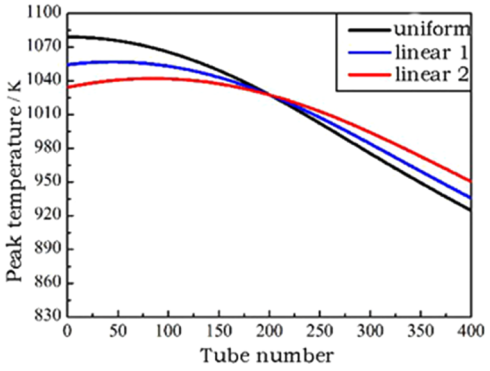

Figure 13. Pipe wall peak temperature distribution under different flow distribution.

of uniform distribution, and the pipe wall temperature is more uniform when the distribution of flow rate is more nonuniform. Moreover, the peak wall temperature is lower when the flow distribution is more nonuniform.

It can be seen from Table 6 that the thermal efficiency and exergy efficiency of the system increase with the increase of the nonuniformity of the flow. In general, the nonuniformity of the flow can improve the ammonia decomposition rate of the system, reduce the peak temperature of the pipe wall, and improve the system efficiency.

4. CONCLUSIONS

In this paper, based on the ammonia energy storage system equipped with the tower solar photovoltaic power generation system, a three-dimensional ammonia decomposition reaction tube model was established according to the energy mass equation, which better reflected the energy and mass transfer characteristics of the ammonia decomposition reaction. After that, the heat absorption side system of ammonia energy storage was built to further study the influence of different working conditions on the energy storage efficiency of the system:

(1) The increase of inlet temperature and the decrease of inlet flow rate are beneficial to the thermal efficiency and exergy efficiency of the system to a certain extent. However, the increase of inlet temperature will lead to the problem that the energy of the reacted gas is not enough to provide enough energy for the supplied ammonia, which will reduce the exergy efficiency. The reduction of inlet flow will also bring more heat to be stored in the form of sensible heat. The heat cannot be effectively converted into chemical energy, the thermal efficiency of the system will decline, and the wall temperature will rise, which will reduce the safety and reliability of the system. Within the scope of simulation in this paper, 573 K, 14 $kg·s^{-1}$ are the optimal working conditions.

(2) The nonuniform flow distribution of the reactor is more conducive to improving the system efficiency and ensuring the safety of the system operation. The nonuniform distribution of the flow can make the place where the energy flow density is concentrated more fully use the heat energy of different sizes at different locations. It can also be found that when the flow distribution is more uneven, the pipe wall temperature is lower and the system efficiency is higher.

AUTHOR INFORMATION

Corresponding Author

Kang Chen − *Institute of Solar Engineering Technology, Northwest Engineering Corporation Limited, PowerChina, Xi'an 710065, China;* orcid.org/0000-0002-9303-5813; Email: chen_kang@mail.xjtu.edu.cn

Authors

Yiming Jin − *State Key Laboratory of Multiphase Flow in Power Engineering, Xi'an Jiaotong University, Xi'an 710049, China*

Table 6. Comparison of System Efficiency Results under Different Flow Distributions

flow distribution	ammonia decomposition rate	thermal efficiency	Exergy efficiency	reactor heat loss (MW)	cooling heat loss (MW)	energy lost by compressor (MW)
uniform distribution	81.85%	70.4%	62.78%	9.956	4.221	4.447
linear distribution 1	82.10%	70.60%	62.96%	10.035	4.004	4.461
linear distribution 2	82.57%	70.97%	63.47%	9.868	3.001	4.486

https://doi.org/10.1021/acsomega.3c02426
ACS Omega 2023, 8, 33321−33331

Huaiwu Peng − *Institute of Solar Engineering Technology, Northwest Engineering Corporation Limited, PowerChina, Xi'an 710065, China*
Pengfei Chen − *Institute of Solar Engineering Technology, Northwest Engineering Corporation Limited, PowerChina, Xi'an 710065, China*
Junfeng Zhang − *Institute of Solar Engineering Technology, Northwest Engineering Corporation Limited, PowerChina, Xi'an 710065, China*
Zhi Zhou − *Institute of Solar Engineering Technology, Northwest Engineering Corporation Limited, PowerChina, Xi'an 710065, China*
Yueshe Wang − *State Key Laboratory of Multiphase Flow in Power Engineering, Xi'an Jiaotong University, Xi'an 710049, China*

Complete contact information is available at: https://pubs.acs.org/10.1021/acsomega.3c02426

Notes

The authors declare no competing financial interest.

■ ACKNOWLEDGMENTS

This research was funded by the Innovation Capability Support Program of Shaanxi (grant no. 2022KJXX-92) and the Key Research and Development Program of Shaanxi (grant no. 2022GY-186).

■ NOMENCLATURE

A	fluid contact area with the tube wall (m^2)
C_p	the specific heat capacity ($J{\cdot}kg^{-1}{\cdot}K^{-1}$)
D_f	fluid diffusion coefficient ($m^2{\cdot}s^{-1}$)
d_p	catalyst particle size (m)
E	exergy ($kJ{\cdot}kg^{-1}$)
E_a	activation energy ($J{\cdot}mol^{-1}$)
H	enthalpy ($kJ{\cdot}kg^{-1}$)
h_{sf}	convective heat transfer coefficient between fluid and pipe wall ($W{\cdot}m^{-2}{\cdot}K^{-1}$)
k_0	reaction rate pre factor, in units consistent with the reaction rate, which here is ($kmol{\cdot}m^{-3}{\cdot}s^{-1}$)
k_p	equilibrium constant
L	pipe length (m)
M	relative molecular mass ($g{\cdot}mol^{-1}$)
n	reversible polytropic index
P	pressure (atm)
P_h	residual energy after mirror focusing (W)
Q_{in}	the energy through solar input into the heat absorption side of the amino energy storage system ($kJ{\cdot}kg^{-1}$)
q_m	mass flow rate of the ammonia decomposition reactor ($kg{\cdot}s^{-1}$)
q_s	heat lost per unit area of the tube wall ($W{\cdot}m^{-2}$)
q_t	heat input per unit area of the pipe wall ($W{\cdot}m^{-2}$)
q_w	thermal energy absorbed by the unit area of the tube wall ($W{\cdot}m^{-2}$)
R	gas constant ($J{\cdot}mol^{-1}{\cdot}K^{-1}$)
R'	ammonia chemical decomposition rate ($kmol{\cdot}m^{-3}{\cdot}s^{-1}$)
T_a	ambient temperature (K)
T_f	fluid temperature (K)
T_{in}	inlet temperature (K)
T_{solid}	catalyst temperature (K)
u_f	flow rate ($m{\cdot}s^{-1}$)
W_{cJ}	compressor power output ($kJ{\cdot}kg^{-1}$)
ΔH	enthalpy change ($kJ{\cdot}kg^{-1}$)
ε	porosity
η_{ex}	exergy efficiency
η_{st}	energy storage efficiency
λ_f	fluid thermal conductivity ($W{\cdot}m^{-1}{\cdot}K^{-1}$)
λ_s	catalyst thermal conductivity ($W{\cdot}m^{-1}{\cdot}K^{-1}$)
μ	fluid viscosity (Pa·s)
ξ	tube wall absorptivity
ρ_f	fluid density ($kg{\cdot}m^{-3}$)
σ	Boltzmann constant
σ_{HF}	deviation coefficient, take 2.5
χ	tube wall emissivity
ω_f	ammonia mass fraction

■ REFERENCES

(1) Lin, B.; Chen, Y. Does electricity price matter for innovation in renewable energy technologies in China? *Energy Economics* **2019**, *78*, 259−266, DOI: 10.1016/j.eneco.2018.11.014.
(2) Răboacă, M. S.; Badea, G.; Enache, A.; Filote, C.; Răsoi, G.; Rata, M.; Lavric, A.; Felseghi, R. A. Concentrating Solar Power Technologies. *Energies* **2019**, *12* (6), 1048 DOI: 10.3390/en12061048.
(3) *China National Bureau of Statistics China Statistical Yearbook[M]*; China Statistics Press, 2022. (in Chinese).
(4) Chen, X.; Zhang, Z.; Qi, C.; Ling, X.; Peng, H. State of the art on the high-temperature thermochemical energy storage systems. *Energy Convers. Manage.* **2018**, *177*, 792−815.
(5) Chen, C. *Ammonia Based Solar Thermochemical Energy Storage System for Direct Production of High Temperature Supercritical Steam*; UCLA, 2017.
(6) Wang, X.; Xuancheng, D.; Jinjia, W. Research progress of different solar Thermochemistry energy storage systems[J]. *Chin. Sci. Bull.* **2017**, *62* (31), 3631−3642.
(7) Carden, P. O. Energy corradiation using the reversible ammonia reaction. *Sol. Energy* **1977**, *19* (4), 365−378.
(8) Williams, O. M.; Carden, P. O. Energy storage efficiency for the ammonia/hydrogen-nitrogen thermochemical energy transfer system. *Int. J. Energy Res.* **1979**, *3*, 29−40, DOI: 10.1002/er.4440030105.
(9) Kanamori, M.; Matsuda, H.; Hasatani, M. Heat Storing/Releasing Characteristics of the Chemical Heat Storing Unit of Electricity Using Ca (OH) 2/CaO Reaction. *Kagaku Kogaku Ronbunshu* **1996**, *22*, 257−263, DOI: 10.1252/kakoronbunshu.22.257.
(10) Meier, A. A predictive CFD model for a falling particle receiver/reactor exposed to concentrated sunlight. *Chem. Eng. Sci.* **1999**, *54* (13), 2899−2905.
(11) Bogdanovi, B.; Reiser, A.; Schlichte, K.; Spliethoff, B.; Tesche, B. Thermodynamics and dynamics of the Mg−Fe−H system and its potential for thermochemical thermal energy storage. *J. Alloys Compd.* **2002**, *345* (1−2), 77−89.
(12) Luzzi, A.; Lovegrove, K.; Filippi, E.; Fricker, H.; Schmitz-Goeb, M.; et al. Techno-economic analysis of a 10 MWe solar thermal power plant using ammonia-based thermochemical energy storage. *Sol. Energy* **1999**, *66*, 91−101, DOI: 10.1016/S0038-092X(98)00108-X.
(13) Lovegrove, K.; Luzzi, A.; Kreetz, H. A solar-driven ammonia-based thermochemical energy storage system. *Sol. Energy* **1999**, *67* (4−6), 309−316.
(14) Lovegrove, K.; Luzzi, A.; Soldiani, I.; Kreetz, H. Developing ammonia based thermochemical energy storage for dish power plants. *Sol. Energy* **2004**, *76* (1−3), 331−337.
(15) Dunn, R. *Receiver Geometries for Solar Dish Concentrators*; ANU, 2016.
(16) Chen, C.; Aryafar, H.; Lovegrove, K. M.; Lavine, A. S. Modeling of ammonia synthesis to produce supercritical steam for solar thermochemical energy storage. *Sol. Energy* **2017**, *155*, 363−371.
(17) Chen, C.; Aryafar, H.; Warrier, G.; Lovegrove, K. M.; Lavine, A. S. *Ammonia Synthesis for Producing Supercritical Steam in the Context of Solar Thermochemical Energy Storage*, Solarpaces: International

Conference on Concentrating Solar Power & Chemical Energy Systems, 2016.
(18) Giuseppe, M.; Carlos, O.; Ricardo, C.; Vittorio, V.; M, V. J. The Ammonia Looping System for Mid-Temperature Thermochemical Energy Storage. *Chem. Eng. Trans.* **2018**, *70*, 763−768.
(19) Abdiwe, R.; Haider, M. *Design of an Ammonia Closed-loop Storage System in a CSP Power Plant with A Power Tower Cavity Receiver*, Solarpaces: International Conference on Concentrating Solar Power & Chemical Energy Systems, 2017.
(20) Long, X.; Kui, L. Thermal performance analysis of amino Thermochemistry energy storage reactor [J]. *Therm. Power Gener.* **2008**, *263* (11), 59−63.
(21) Villafán-Vidales, H.; Abanades, S.; Caliot, C.; Romero-Paredes, H. Heat transfer simulation in a thermochemical solar reactor based on a volumetric porous receiver. *Appl. Therm. Eng.* **2011**, *31* (16), 3377−3386.
(22) Wang, F.; Shuai, Y.; Wang, Z.; Leng, Y.; Tan, H. Thermal and chemical reaction performance analyses of steam methane reforming in porous media solar thermochemical reactor. *Int. J. Hydrogen Energy* **2014**, *39*, 718−730, DOI: 10.1016/j.ijhydene.2013.10.132.
(23) Tamaru, K. A ″new″ general mechanism of ammonia synthesis and decomposition on transition metals. *Acc. Chem. Res.* **1988**, *21*, 88−94, DOI: 10.1021/ar00146a007.
(24) Jennings, J. R. *Catalytic Ammonia Synthesis*; Springer: US, 1991.
(25) Chen, X.; Li, X.; Xia, X.; Sun, C. Effects of radiation on the coupled heat transfer in a high temperature tube filled with porous media. *J. Aerospace Power* **2016**, *31* (10), 2437−2442.
(26) Amiri, A.; Vafai, K.; Kuzay, T. M. Effects of Boundary Conditions on Non-Darcian Heat Transfer Through Porous Media and Experimental Comparisons. *Numer. Heat Transfer* **1995**, *27* (6), 651−664.
(27) Wakao, N. Particle-to-fluid transfer coefficients and fluid diffusivities at low flow rate in packed beds. *Chem. Eng. Sci.* **1976**, *31* (12), 1115−1122.
(28) E, R. *Thermodynamic and Transport Properties*. Wiley, 1997.

https://doi.org/10.1021/acsomega.3c02426
ACS Omega 2023, 8, 33321−33331